

Spatiodynamic Inference Using Vision-Based Generative Modeling

Jun Won Park, Kangyu Zhao, Sanket Rane *

Irving Institute for Cancer Dynamics, Columbia University, New York, USA

Abstract

Biological systems commonly exhibit complex spatiotemporal patterns whose underlying generative mechanisms pose a significant analytical challenge. Traditional approaches to spatiodynamic inference rely on dimensionality reduction through summary statistics, which sacrifice complexity and interdependent structure intrinsic to these data in favor of parameter identifiability. This imposes a fundamental constraint on reliably extracting mechanistic insights from spatiotemporal data, highlighting the need for analytical frameworks that preserve the full richness of these dynamical systems. To address this, we developed a simulation-based inference framework that employs vision transformer-driven variational encoding to generate compact representations of the data, exploiting the inherent contextual dependencies. These representations are subsequently integrated into a likelihood-free Bayesian approach for parameter inference. The central idea is to construct a fine-grained, structured mesh of latent representations from simulated dynamics through systematic exploration of the parameter space. This encoded mesh of latent embeddings then serves as a reference map for retrieving parameter values that correspond to observed data. By integrating generative modeling with Bayesian principles, our approach provides a unified inference framework to identify both spatial and temporal patterns that manifest in multivariate dynamical systems.

*Corresponding Author: sanket.rane@columbia.edu

Introduction

Spatiotemporal patterns are ubiquitous in biological systems whose mechanistic underpinnings present a significant analytical challenge. Spatial dynamical data exhibit multi-scale dependencies among observed variables, encompassing both local and global relationships. Mathematical models are a natural language for describing such interconnectedness and for inferring causal relationships. However, the accuracy of their conclusions hinges on precisely identifying model parameters (θ) and quantifying the uncertainty in their estimation using the observed data (y).

In Bayesian regimes, this involves determining the posterior distribution $\pi(\theta|y)$ given the prior $\pi(\theta)$ and the likelihood function $p(y|\theta)$. In cases where traditional likelihood-based methods are impractical, approximate Bayesian Computation (ABC) offers an appealing solution to estimating posterior using simulated data¹⁻³. ABC and its modern variants⁴⁻⁷ use a distance metric, $\rho(\cdot)$, to gauge the similarity between simulated and observed datasets and a threshold ϵ to accept posterior samples (**eq. 1**), such that, as $\epsilon \rightarrow 0$, ABC posterior approaches the Bayesian posterior.

$$\pi(\theta|Y = y^{obs}) \approx \pi(\theta | \rho(y^{sim}, y^{obs}) \leq \epsilon) \quad (1)$$

Inference on spatial data typically involves mixed models, consisting a regression model for covariates and a random-effects model, such as the Gaussian process, for spatial dependence⁸⁻¹³. In many studies, specifically in epidemiology, summarized statistics are leveraged to estimate model parameters using Bayesian methods¹⁴⁻¹⁶. Formulating meaningful summary statistics becomes increasingly difficult when working with high-dimensional spaces, frequently resulting in ill-posed inverse problems where parameter identifiability is compromised. These factors critically impede reliable mechanistic inference on spatiotemporal dynamics, highlighting the need for more sophisticated approaches that preserve the full richness of these data.

To bridge this gap, we defined an integrative approach that combines a generative deep learning model with ABC to infer the underlying data-generating process and assess uncertainty in its parameter estimation. We begin with a simple hypothesis that complex observed data contain underlying simpler patterns that are unobserved. These hidden patterns can yield significant insights regarding the parameters that govern dynamical or mechanistic variations within the data. Our objective is to construct a structured mesh of latent representations of simulated data by systematically drawing samples from the prior. This reference map will then be employed in a Bayesian framework to extract model parameters corresponding to the actual observations.

We developed a variational inference-assisted ABC (viaABC) framework by integrating elements of Vision Transformer (ViT) and variational autoencoding (VAE) to construct the reference map of latent representations. viaABC begins with a self-supervised training phase on synthetic data generated using parameter samples drawn from model-agnostic, weakly informative priors. The trained encoder is integrated into a simulation-based inference framework to systematically com-

pare the latent representations of observed data with those generated from simulations of the mechanistic model (eq. 2) using an adaptive acceptance criterion¹⁷. Through this process, viaABC approximates the posterior distribution of the parameters that underlie the observed dynamics,

$$\pi(\theta|y = y^{obs}) \approx \pi(\theta|\rho(\zeta(y^{sim}), \zeta(y^{obs})) \leq \epsilon), \quad (2)$$

where $\zeta(\cdot)$ represents variational encoding process that generates the latent variables.

Toy example: The spatial SIRS model

Infectious disease spread is characterized by complex spatiotemporal patterns^{18–20}, which can be modeled through spatial adaptations of the susceptible-infected-recovered (SIR) model²¹. To assess latent-ABC’s ability to conduct mechanistic inference on spatial dynamical data, we employed a grid-structured contact network spatial SIR model as developed by van Ballegooijen *et al.*²². This framework utilized a modification of the classical SIR, known as the SIRS model²³, in which individuals occupy one of three states: susceptible (S), infected (I), or resistant (R) (**Fig. 1A**).

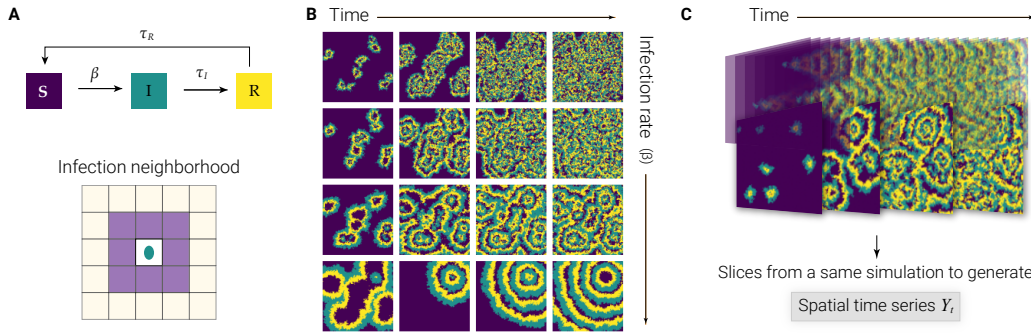


Figure 1: Spatial dynamics of the SIRS model. **A.** Schematic of the state transitions. In addition, we depict the contact-grid for each individual (pixel), which serves as the infection neighborhood. **B.** An illustration of the varied patterns generated by the SIRS model. This particular example depicts the output of SIRS model at times $t = 4, 8, 12, 16$ (left to right) by fixing $\tau_I = \tau_R = 1$ and varying $\beta = 0.4, 0.7, 1.0, 2.0$ (top to bottom). Such diversity allows us to train the deep learning model on a wide assortment of spatiotemporal patterns, which we generate by sampling θ from a model agnostic prior distribution. **C.** Schematic of data generation and processing. We simulate the SIRS model using the time-step of 0.05 and slice the generated video at every 20th step to construct the spatial time series.

Within this model, infected individuals stochastically transmit the infection to neighboring susceptible individuals at the rate β . The infection neighborhood is represented by eight adjacent individuals on a square lattice (**Fig. 1A**). The duration of the infectious period is fixed at τ_I , following which the infected individuals transition to the resistant state. Subsequently, resistant individuals revert to the susceptible state after a fixed time period τ_R . We adhered to the methodology outlined in van Ballegooijen *et al.*²², scale τ_R to unity and sought to infer $\theta = (\beta, \tau_I)$, using our framework. The SIRS model produces well-defined spatiotemporal patterns—from scattered clusters to infection waves—that are clearly delineated by its parameters (**Fig. 1B**) and, as such, provides an excellent test case for evaluating viaABC’s performance. We generated a synthetic

dataset by fixing $\theta = (1.0, 1.0)$ as the ground truth. We sampled 15 slices of images from this dataset to create a test dataset (schematic shown in **Fig. 1B**), which we refer to as the ‘observed data’ (y^{obs}). We generated the training data for VAE similarly (see methods for details).

Cosine similarity of the latent variables as an acceptance criterion

We postulate that contextual relationship between data points and patterns hidden within the data generating processes could be realized by projecting simulations and observed data to latent variables. Such projections could precisely inform on model parameters and may also help in model validation and selection procedures. To facilitate this we propose to use closeness between latent variables of the observed and simulated data, which we evaluate using patch-wise cosine similarity, as an acceptance criterion (**Fig. 2**).

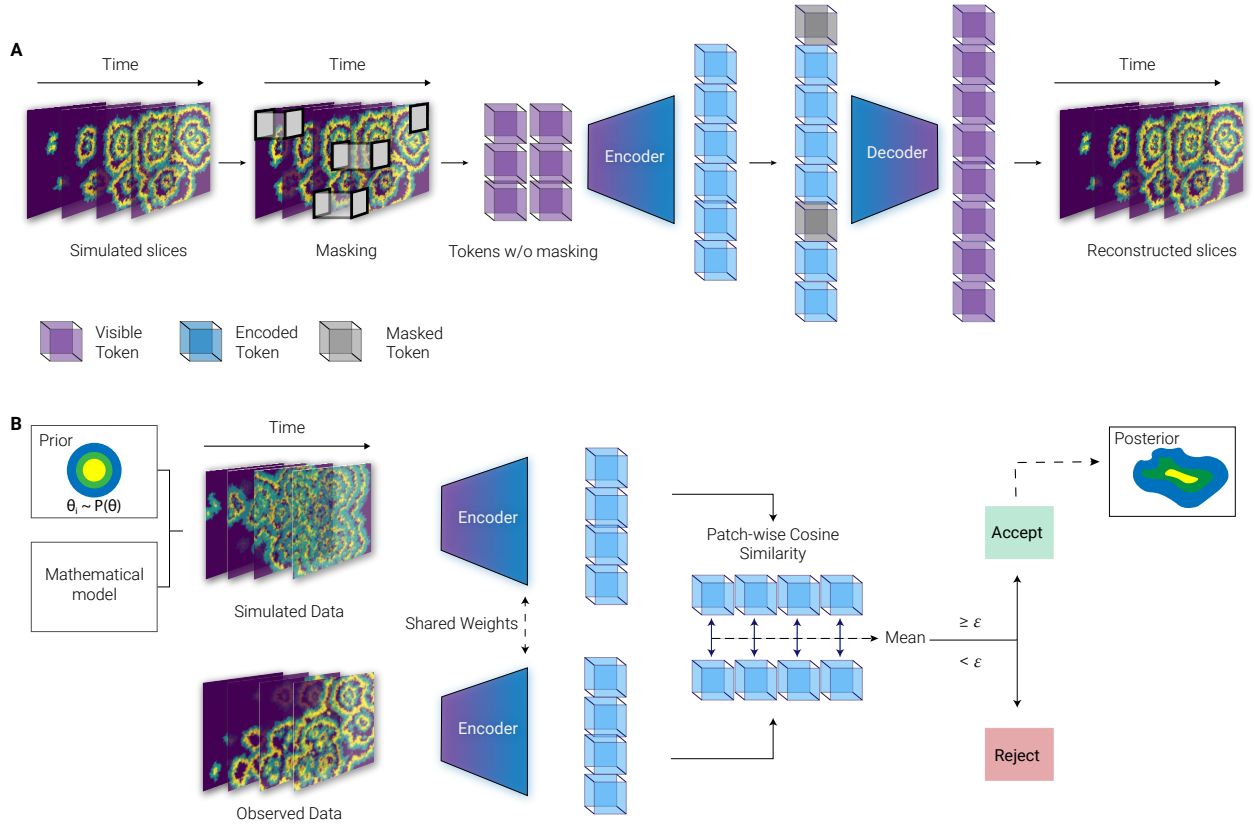


Figure 2: Schematic of the viaABC framework. We depict viaABC operation for spatial dynamical data relevant to the SIRS model. **A. Training:** Each training sample consists of a sequence of simulated images or data slices. Each slice is divided into multiple non-overlapping regions called patches. We group patches along the time dimension to form cubes, which are then flattened into vectorized representation called tokens. Within each training sample, a random subset of tokens is masked. VAE is trained to reconstruct the original data using tokens as the input, while minimizing the KL divergence loss in the latent space. Encoder is applied to only visible tokens (purple). Encoded tokens (blue) are probabilistically sampled and along with the mask tokens (gray) are then processed by a decoder. **B. Inference:** Trained encoder is applied to the unmasked data, both simulated and observed, to infer model parameters using sequential Monte Carlo and patch-wise cosine similarity as an acceptance criterion. We exclude the decoder and sampling process from the inference procedure. Principles of training and inference remain same across all data types and architectures described in this study.

We customized a VAE model by adopting the transformer-based masked autoencoder²⁴ and imposing a probability distribution in the latent space via Kullback–Leibler (KL) divergence. The resultant loss function is,

$$L = L_{\text{recon}} + \lambda L_{KL}, \quad (3)$$

where L_{recon} is the reconstruction loss, L_{KL} denotes the KL divergence loss. The hyperparameter λ mediates the trade-off between L_{recon} and L_{KL} ²⁵. Our approach considers the loss in reconstruction for both unmasked and masked patches, deviating from conventional masked modeling approaches that only rely on masked patches.^{26–28} In addition, we only use the encoded tokens to calculate the KL divergence loss (**Fig. 2A**).

To generate the training data we draw N parameter sets from a joint prior distribution using Latin hypercube sampling (LHS). We chose LHS as it provides a thorough exploration of the parameter space resulting in a diverse range of parameter configurations²⁹. Further, we use wide uniform priors for the training procedure to mitigate the risk of overfitting to specific modes in the parameter space. Given a mathematical model or data-generating process f , this procedure yields N pairs of $\{(\theta_i, f(\theta_i))\}_{i=1}^N$. Masked VAE is trained on $\{f(\theta_i)\}_{i=1}^N$ to reconstruct the input data while minimizing the total loss L (**Fig. 2A**).

We define ABC posterior following the notations of Marin et al.³⁰ and Simola et al.¹⁷ as,

$$\pi_\epsilon(\theta|y^{\text{obs}}) = \int \left[\frac{p(y^{\text{sim}}|\theta)\pi(\theta)\mathbb{1}_{A_{\epsilon,y^{\text{obs}}}}(y^{\text{sim}})}{\int_{A_{\epsilon,y^{\text{obs}}} \times \Theta} p(y|\theta)\pi(\theta)dy^{\text{sim}}d\theta} \right] dy^{\text{sim}},$$

where $\mathbb{1}_{A_{\epsilon,y^{\text{obs}}}}(\cdot)$ is the indicator function for the set $A_{\epsilon,y^{\text{obs}}} = \{y^{\text{sim}}|\rho(s(y^{\text{obs}}), s(y^{\text{sim}})) \leq \epsilon\}$, $\rho(\cdot, \cdot)$ is the distance function and $s(\cdot)$ is the summary statistic function.

In viaABC, we modify the set notation such that,

$$A_{\epsilon,y^{\text{obs}}} = \{y^{\text{sim}}|\rho(z^{\text{obs}}, z^{\text{sim}}) \leq \epsilon\},$$

where z^{obs} and z^{sim} are latent embeddings of the observed and simulated data outputted by the combination of the encoder and re-parameterization layers. The re-parameterization layer imposes a standard Gaussian distribution in the latent space through,

$$Z = \mu + \sigma\epsilon, \quad \epsilon \sim \mathcal{N}(0, I), \quad (4)$$

which then outputs mean μ_i and standard deviation σ_i vectors for each token i . Both the decoder and sampling process are excluded from the inference procedure and only the vector of means μ is considered (**Fig. 2B**) such that the latent representation $Z = \mu$ (**eq. 4**). We use patch-wise cosine distance metric to compute the distance between latent embeddings (**Algorithm 1 Line 6**), (**Fig. 2B**). For each pair of corresponding patches in z^{obs} and z^{sim} , we compute cosine similarity

and aggregate across all n patches such that

$$\rho(z^{sim}, z^{obs}) = 1 - \sum_{i=1}^n \frac{z_i^{obs} \cdot z_i^{sim}}{\|z_i^{obs}\|_2 \|z_i^{sim}\|_2} \quad (5)$$

where $Z \in \mathbb{R}^{n \times E}$, where E is the embedding dimension of the decoder. Sampled parameters are accepted based on the patch-wise cosine distance metric (eq. 5).

Parameter inference from learned representations of spatiotemporal input

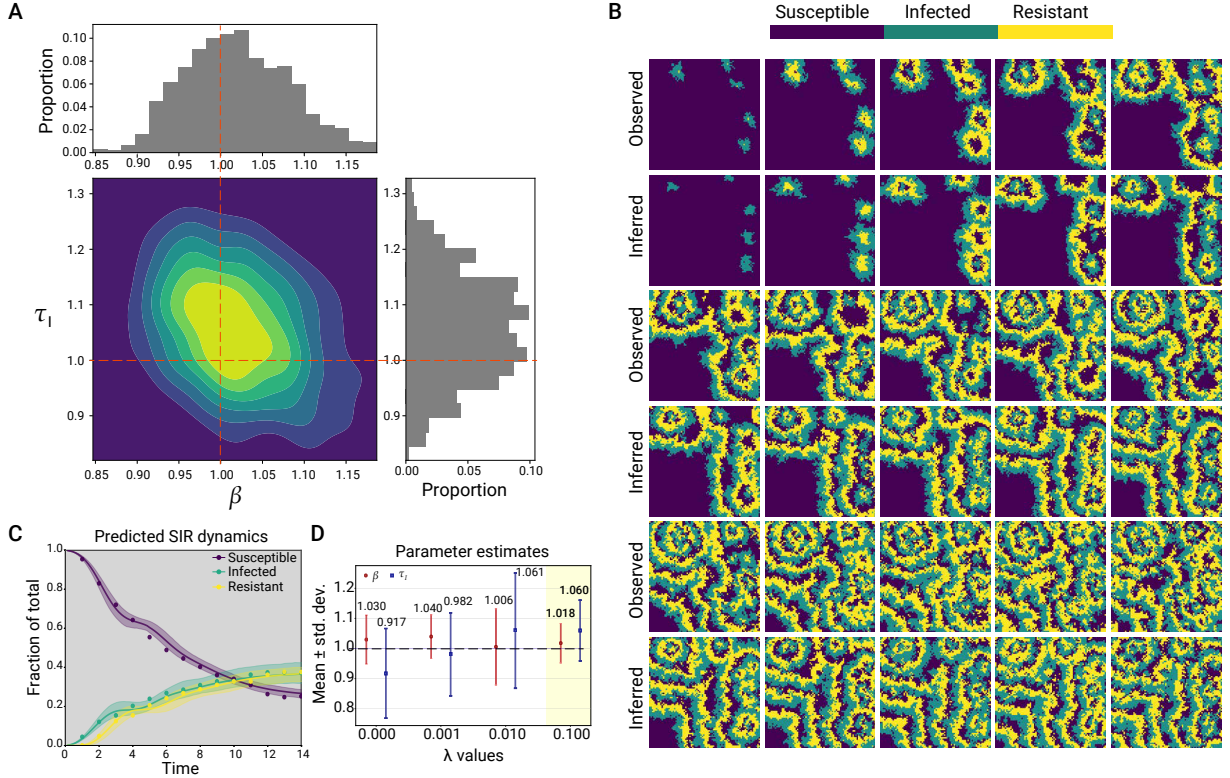


Figure 3: Posterior inference on spatial SIRS dynamics using viaABC. **A.** Kernel density estimate of the final particles for the parameters β and τ_I . **B.** Comparison of spatiotemporal dynamics of the observed data and predictions generated using the mean parameter estimates. Predictions were initialized within the similar region on the spatial grid as that of the observed data (see Methods for details). **C.** SIRS dynamics aggregated across spatial dimensions. We average the proportions of S, I, and R at each time point across 10 simulations generated from each posterior draw. Dots represent observed data. Lines denote the mean of predictions, and envelopes are 95% credible intervals. **D.** Mean estimates and corresponding standard deviations, calculated from five independent experiments for each λ value. Results from ViT-VAE trained with $\lambda = 0.1$ are highlighted in yellow. Dashed line represent the ground truth. Note that $\lambda = 0$ corresponds to the standard MAE.

We employed viaABC to estimate the parameters ($\theta = (\beta, \tau_I)$) of the spatial SIRS model using synthetically generated observed data (Fig. 1C). We sampled β and τ_I from a bivariate Unif(0, 4.2) using LHS and generated 50,000 simulations for training and an additional 10,000 simulations for validation. Each simulation contains 15 time points, with each time point representing a tensor

of dimension $3 \times 80 \times 80$. Here 80×80 denotes the spatial grid and the first dimension encodes the state of each individual. The three channels reflect distinct states—susceptible, infected, or resistant—encoded in a binary format; for instance, each individual is denoted by a 1 in the second channel if infected, otherwise 0. As the datatype only contained discrete labels, we formulated the reconstruction loss as cross-entropy loss.

The VAE architecture comprised a ViT based encoder with 6 layers and an embedding dimension of 128, and a smaller ViT based decoder with 4 layers and an embedding dimension of 64. The input data of size $3 \times 15 \times 80 \times 80$ is divided into non-overlapping spatio-temporal cubes of size $3 \times 3 \times 10 \times 10$, yielding 500 cubes. Each cube is flattened to form a token, 15% of which are randomly masked during training (as depicted in **Fig. 2B**). We set $\lambda = 0.1$ in **eq. 3** to calculate the loss and train the VAE. We used the trained encoder and same prior as before to perform the posterior inference. viaABC iteratively and adaptively accepted 1,000 independent particles until the stopping rule of $q_t = 0.99$ or $t \geq 20$ was satisfied (as described in **Algorithm 1**).

The posterior inferred through viaABC contained the ground truth, and the estimated mean $\hat{\theta} \approx (1.04, 0.98)$ nearly coincided with $\theta = (1, 1)$ (**Fig. 3A and D**). Consistent with this, the predicted spatial SIR dynamics, generated using the mean of the posterior, closely mirrored the observed data (**Fig. 3B**). We further show that the summarized SIRS dynamics generated using posterior draws nicely captured the summary statistics of the observed data (**Fig. 3C**). Lastly, we explored the effects of varying λ on accuracy of the posterior inference. We present the aggregated results across five independent experiments in (**Fig. 3B**). For all configurations, the 95% highest density interval (HDI) from the posterior inference included the ground truth, suggesting that viABC is rather weakly sensitive to fluctuations in the regularization parameter λ . Notably, all VAE configurations improved on the results from the autoencoder version (**Fig. 3D**) and, on average, converged more efficiently, indicating a more structured latent space.

Inference on noisy dynamical input

Next, we assessed and compared the efficacy of the viaABC algorithm in a non-spatial setting. We used the Lotka-Volterra model^{31,32}, a classic system in ecology, which deterministically describes the population dynamics and interactions between a prey (x) and predator (y) species. This system is expressed as a pair of nonlinear differential equations,

$$\frac{dx}{dt} = ax - cxy, \quad \frac{dy}{dt} = bxy - dy, \quad (6)$$

where a and b denote rates of population growth of the prey and their per capita loss due to predation. Parameters c and d represent the efficiency with which consumed prey are converted into predator offspring and loss of the predators, respectively. The Lotka-Volterra model is a well-studied system, and its parameters have been estimated using various methods, including ABC^{6,33}, ABC with distributional Random Forest (ABC-DRF)³⁴, and ABC with deep learning

(ABC-DL)^{35–37}. We adhered to the methodology outlined in Toni⁶ and Dinh³⁴ *et al.*, fixed parameters $c = d = 1$ and sought to infer $\theta = (a, b)$ using the prior $a, b \sim \text{Uniform}(0, 10)$.

We generated $N = 50,000$ training simulations and 20,000 validation samples of prey, predator dynamics (shown as lines in **Fig. 4A**), by sampling θ from the joint prior distribution using LHS. We selected eight time points between $t = 0$ and 15 to represent our training data $s^{\text{train}} = \{\{x_1^i, y_1^i, \dots, x_8^i, y_8^i\}\}_{i=1}^N$. The input data of size 2×8 is divided into 8 non-overlapping patches of size 2×1 . We trained the ViT-VAE using a masking ratio of 15%. The comparison between reconstructions of masked and unmasked training data shows that our ViT-VAE effectively imputes missing observations using the patterns within the training data (**Fig. S1**).

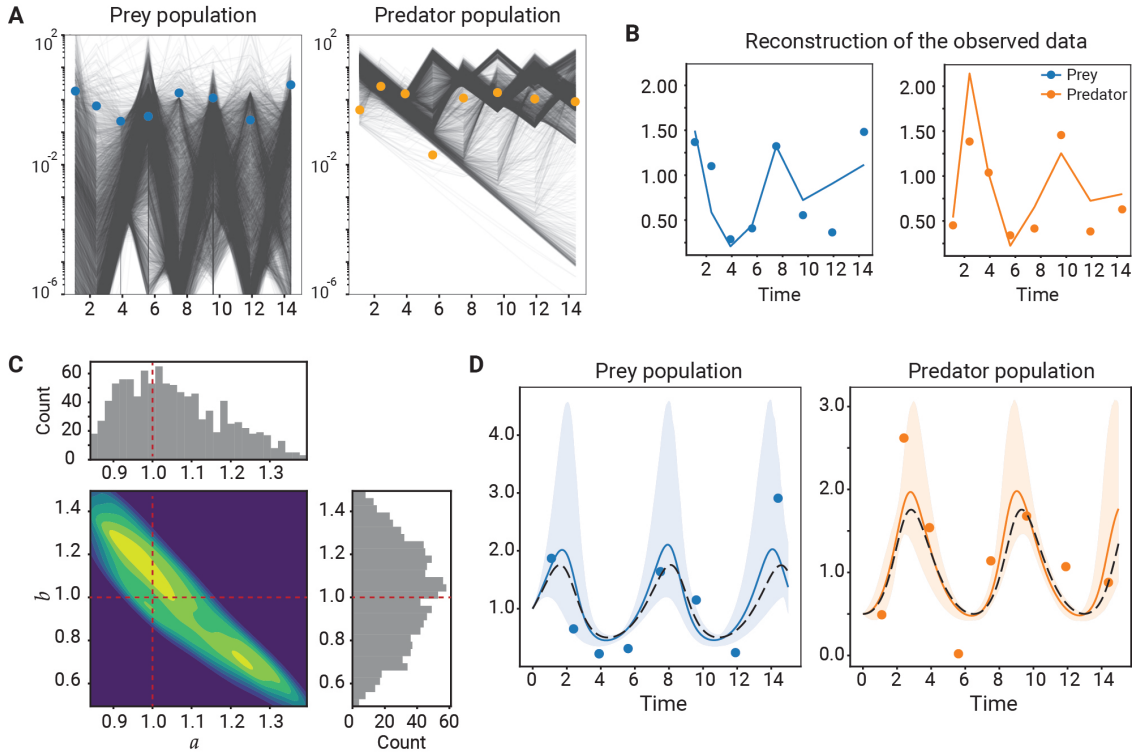


Figure 4: Learning and inferring predator-prey dynamics. **A.** The simulated dynamics of the training data, denoted as lines, and the observed data, denoted as dots. Y-axis is on the log scale to fully visualize the wide range of predator-prey dynamics in the simulated data. **B.** ViT-VAE’s reconstructions (lines) of the noisy observed data (dots). **C.** The kernel density estimated 2D heatmap of the final posteriors along with their histograms. The ground truth is denoted as dotted red lines. The estimated 95% HDI for a, b are (0.951, 1.188) and (0.768, 1.352), respectively. **D.** The 95% credible intervals of the predictions of prey, predator dynamics with medians as solid lines. Black dashed lines denote predator-prey dynamics generated using the ground truth without the Gaussian noise.

To construct the observed data, we evaluated x, y using eq. 6 at the same eight time points as the training samples and by setting $(\theta = (1, 1))$, see methods for details). Gaussian noise $\epsilon_t \sim \mathcal{N}(0, 0.5^2)$ was added to this time series to represent experimental variation typically associated with biological samples. This forms our noisy dynamical input $s^{\text{obs}} = \{x_1^o, y_1^o, \dots, x_8^o, y_8^o\}$ (shown as dots in **Fig. 4A**), which we used as the observed data for simulation-based inference. In **Fig. 4B**, we show the reconstruction of the s^{obs} (original data as dots, reconstructed as lines).

To generate simulated data for parameter inference, we sampled θ from the bivariate uniform prior to simulate time series $s^{\text{sim}} = \{x_1^s, y_1^s, \dots, x_8^s, y_8^s\}$. Both, observed simulated data are then encoded into their respective latent variables and were used to infer posterior of θ using viaABC. Specifically, We accepted 1,000 particles based on the cosine similarity of z^{sim} to z^{obs} . This procedure is repeated until the stopping rule described in the **Algorithm 1** is satisfied.

We observed that the ground truth $\theta = (1, 1)$ lied within the high density region of the posterior of the accepted particles, very close to the estimated $\hat{\theta} \approx (1.06, 1.06)$ (**Fig. 4C**). We further show that the 95% credible intervals of the predictions of prey, predator dynamics contains the data generated using the ground truth and the median of the interval closely overlaps with the observed data (**Fig. 4D**). Lastly, we benchmarked our approach against other Monte Carlo-based approaches and found that viaABC delivered results comparable to well-known Bayesian algorithms (**Table 1**) and produced lowest uncertainty in parameter estimation.

Statistics	viaABC	MCMC	ABC-SMC-DRF	ABC-SMC
$\mathbb{E}(\text{a})$	1.064	1.087	1.121	1.291
$\text{Var}(\text{a})$	0.005	0.006	0.033	0.110
$\mathbb{E}(\text{b})$	1.057	1.100	0.970	1.026
$\text{Var}(\text{b})$	0.029	0.034	0.031	0.104

Table 1: Means and variances of marginal posterior distributions of the parameters of the Lotka-Volterra model. We compared the estimates obtained using viaABC with Markov Chain Monte Carlo (MCMC) sampler (produced using *stan* programming language and same priors, results shown in (**Fig. S2**), ABC-SMC and ABC-SMC-DRF (results directly taken from Dinh *et al*³⁴). Expectations closest to the ground truth and lowest variances are highlighted in bold.

Discussion

In this study we introduced viaABC, a simulation-based inference framework that uses contextual dependencies inherent in the data to estimate parameters of multivariate dynamical systems. The framework employs a vision transformer-based masked variational autoencoder to create ordered latent representations of model simulations, where simulations with similar dynamics are positioned close together in the embedding space. The key insight is that by systematically exploring the parameter space, viaABC builds a comprehensive reference library of simulated dynamics that helps to identify which parameters most likely generated the patterns we see in the observed data. We demonstrated efficacy of this approach using the spatial stochastic SIRS system, which exhibits complex dependencies between spatial dimensions and across time, where viaABC accurately retrieved model parameters and quantified the uncertainty in their estimation.

Variational encoding confers viaABC the ability to accommodate datasets with diverse structures and dimensions, as VAE can be employed to compress or expand data dimensions as needed for parameter inference. This can significantly reduce the computational burden typically associated with large data structures, making viaABC aptly suitable for multidimensional data. For instance, calculating the likelihood based on Poisson distribution over an 80 by 80 grid and across

a time series in traditional Bayesian approaches would require heavy computation and becomes increasingly challenging at higher resolutions and longer timescales. Likelihood-free ABC-based approaches handle the computational burden through the implementation of low dimensional summary statistics for high-dimensional data structures. Nevertheless, the efficacy of these approaches is contingent upon the judicious selection of summary statistics and compatible distance metrics. Automating this selection process has been the subject of an intense study.

Fearnhead and Prangle were among the first to effectively bypass the need for selecting summary statistics in ABC³⁸. They demonstrated that the posterior mean of parameters serves as an optimal summary statistic under quadratic loss and introduced a regression-based method for its estimation. Building on this foundation, Jiang *et al.*³⁵ employed dense neural network layers, while Akesson *et al.*³⁶ used convolutional neural networks (CNN) to encode the posterior mean within the hidden layers of their architectures before incorporating it as a summary statistic in ABC frameworks. Notably, Wang *et al.*³⁹ leveraged a VAE model to automate summary statistic selection. Specifically, they derived latent variables (z^{sim}) from a small sample of simulated data and then used a support vector regression model to link θ and z^{sim} , treating the latter as response variables. Predicted z_i^{sim} for each sampled θ_i were then used for parameter inference.

Our approach differs fundamentally from the studies described above in its learning objective. Rather than approximating the posterior mean, viaABC is designed to create regularized and meaningful latent representations while reconstructing the original data. This design philosophy aligns closely with the *manifold hypothesis*—the principle that the underlying structure of high dimensional data resides within low dimensional manifolds embedded within the high dimensional space. Moreover, our model architecture provides a key advantage that it can encode and analyze both spatial and temporal information within a single, unified inference framework, leveraging the inherent capabilities of the vision transformer. In contrast, the previously described approaches are typically designed to handle either spatial or temporal data exclusively. Although a sequential CNN that first extracts spatial features before modeling temporal dynamics could theoretically achieve comparable results.

Lastly, we demonstrated viaABC’s ability to leverage contextual dependencies beyond spatial contexts. We showed that viaABC achieved results comparable to established Bayesian algorithms when estimating parameters of the Lotka-Volterra predator-prey model using sparse, noisy data. In future work, we will expand our framework to enable comparison and ranking of mathematical models. We propose implementing hierarchical architectures that encode simulations from independent models within a single, categorized latent space. The resulting ensemble representations of simulated dynamics across all candidate models can, in principle, be leveraged to derive model-averaged predictions and compute model weights in conjunction with parameter inference.

Methods

Data generation for the SIRS model:

We simulated the spatial SIRS model using predefined initial conditions on an 80×80 grid, where each cell represents an individual. Across all simulations, we chose five infection hotspots within the grid. The model is initialized at $t = 0$ with an infected individual in the vicinity of each infection hotspot. The exact locations of initial infections in each simulation was varied stochastically by sampling from a uniform distribution over $(-5,5)$ in each direction. Susceptible individuals get infected with the following probability $P(\text{Infected} \mid \text{Susceptible}) = 1 - e^{-\beta \cdot i \cdot \Delta t}$, where i is the number of infected neighbors and Δt is the simulation time step. An infected individual recovers from an infection after a fixed period τ_I and a recovered individual remain resistant to new infection for τ_R time period, which was fixed to be 1.0. For simulations and inference, we use general priors $Unif(0, 4.3)$ for both β and τ_I , and set the stepsize $\Delta t = 0.05$. Generated video is then sliced into images taken at every 20 steps form the training data. We generate the observed data using same procedure at β and $\tau_I = (1.0, 1.0)$.

Data generation and scaling for the Lotka-Volterra model:

We simulated the Lotka-Volterra model using fixed initial conditions of $(x, y) = (1, 0.5)$. For training, the parameters a and b were sampled from uniform priors, $a, b \sim Unif(0, 10)$, using Latin Hypercube Sampling (LHS). The model was numerically integrated using the *RK45 ODE solver* in *python*. Variation between data scales in multivariate time series presents optimization challenges for deep learning models. Data normalization is thus a crucial pre-processing step to ensure stable training. A widely used normalization approach involves applying an affine transformation to the time series, i.e.. $\tilde{x} = (x_i - m)/s$ ^{40,41}. We employed mean scaling by setting $m = 0$ and $s = \frac{1}{n} \sum_{i=1}^n |x_i|$ for both simulated and observed data generated using the Lotka-Volterra model, as it has demonstrated effectiveness in deep learning models frequently applied to practical time-series tasks⁴⁰⁻⁴². During inference, parameter values were drawn from the same uniform priors, but without LHS sampling.

Code availability: Code containing model definitions, training scripts, inference scripts, and notebooks used to generate our figures for reproducibility is available in a GitHub repository archived on Zenodo: <https://zenodo.org/records/15776261>.

Algorithm 1 viaABC: Variational Inference Assisted Approximate Bayesian Computation

1: **Given:**

$\zeta(\cdot)$: a trained encoder

T : total number of iterations for termination

N : number of accepted particles per iteration

k : multiplier for the initial sampling pool ($k > 1$)

q : final quantile threshold for termination

z^{obs} : encoded observed data, i.e., $z^{\text{obs}} = \zeta(y^{\text{obs}})$

Initialization ($t = 1$):

2: **for** $i = 1$ to kN **do**

3: Sample: $\theta_i^{(1)} \sim \pi(\theta)$

4: Simulate: $y^{\text{sim}} \sim f(y \mid \theta_i^{(1)})$

5: Encode: $z_i^{\text{sim}} = \zeta(y^{\text{sim}})$

6: Compute distance: $d_i = \rho(z^{\text{obs}}, z_i^{\text{sim}})$

7: **end for**

8: Let $D = \{d_i\}_{i=1}^{kN}$ and sort D in increasing order

9: Re-order particles $\{\theta_i^{(1)}\}_{i=1}^{kN}$ accordingly to D

10: Set initial tolerance $\epsilon_1 = d_{(N)}$ (the N th smallest value in D)

11: Set initial particles: $\{\theta_i^{(1)}\}_{i=1}^N$

Iterations ($2 \leq t \leq T$):

12: **for** $t = 2$ to T **do**

13: Compute weighted empirical variance: $\tau_{t-1}^2 = 2 \cdot \text{Var}_\omega \left(\{\theta_i^{(t-1)}\}_{i=1}^N \right)$

14: **for** $i = 1$ to N **do**

15: **repeat**

16: Sample $\theta^* \sim \{\theta_j^{(t-1)}\}_{j=1}^N$ with weights $\{\omega_j^{(t-1)}\}_{j=1}^N$

17: Perturb: $\theta_i^{**} \sim \mathcal{N}(\theta^*, \tau_{t-1}^2)$

18: Simulate $y^{\text{sim}} \sim f(y \mid \theta_i^{**})$

19: Encode: $z^{\text{sim}} = \zeta(y^{\text{sim}})$

20: Compute distance: $d = \rho(z^{\text{obs}}, z^{\text{sim}})$

21: **until** $d \leq \epsilon_{t-1}$

22: Record distance: $d_i^{(t)} = d$

23: Record particle: $\theta_i^{(t)} = \theta^{**}$

24: Update weight:

$$\omega_i^{(t)} \propto \frac{\pi(\theta_i^{(t)})}{\sum_{j=1}^N \omega_j^{(t-1)} \cdot \phi\left(\theta_i^{(t)}; \theta_j^{(t-1)}, \tau_{t-1}^2\right)}$$

where $\phi(\cdot; \mu, \sigma^2)$ is the normal density function

25: **end for**

-
- 26: Normalize weights such that $\sum_{i=1}^N w_i^{(t)} = 1$
27: Estimate normalizing constant:

$$\hat{c}_t = \sup_{\theta} \frac{\pi_{\epsilon_t}(\theta)}{\pi_{\epsilon_{t-1}}(\theta)}$$

- 28: Update quantile level: $q_t = \frac{1}{\hat{c}_t}$
29: Update tolerance: $\epsilon_t = \text{Quantile}(\{d_i^{(t)}\}_{i=1}^N, q_t)$
30: **if** $q_t \geq q$ **then**
31: **Break**
32: **end if**
33: **end for**
-

Cited literature

1. Donald B. Rubin. Bayesianly justifiable and relevant frequency calculations for the applied statistician. *The Annals of Statistics*, 12(4), December 1984.
2. Peter J. Diggle and Richard J. Gratton. Monte carlo methods of inference for implicit statistical models. *Journal of the Royal Statistical Society. Series B (Methodological)*, 46(2):193–227, 1984.
3. Simon Tavaré, David J Balding, Robert C Griffiths, and Peter Donnelly. Inferring coalescence times from dna sequence data. *Genetics*, 145(2):505–518, 1997.
4. S. A. Sisson, Y. Fan, and Mark M. Tanaka. Sequential monte carlo without likelihoods. *Proceedings of the National Academy of Sciences*, 104(6):1760–1765, February 2007.
5. Paul Marjoram, John Molitor, Vincent Plagnol, and Simon Tavaré. Markov chain monte carlo without likelihoods. *Proceedings of the National Academy of Sciences*, 100(26):15324–15328, 2003.
6. Tina Toni, David Welch, Natalja Strelkowa, Andreas Ipsen, and Michael PH Stumpf. Approximate bayesian computation scheme for parameter inference and model selection in dynamical systems. *Journal of the Royal Society Interface*, 6(31):187–202, 2009.
7. Christian P Robert, Mark A Beaumont, Jean-Michel Marin, and Jean-Marie Cornuet. Adaptivity for abc algorithms: the abc-pmc scheme. *arXiv preprint arXiv:0805.2256*, 2008.
8. Noel Cressie, Matthew Sainsbury-Dale, and Andrew Zammit-Mangion. Basis-function models in spatial statistics. *Annual Review of Statistics and Its Application*, 9(1):373–400, March 2022.
9. Emily L. Kang and Noel Cressie. Bayesian inference for the spatial random effects model. *Journal of the American Statistical Association*, 106(495):972–983, September 2011.
10. Wentao Zhan and Abhirup Datta. Neural networks for geospatial data. *Journal of the American Statistical Association*, 120(549):535–547, June 2024.

11. Arkajyoti Saha, Sumanta Basu, and Abhirup Datta. Random forests for spatially dependent data. *Journal of the American Statistical Association*, 118(541):665–683, August 2021.
12. Abhirup Datta, Sudipto Banerjee, Andrew O. Finley, and Alan E. Gelfand. Hierarchical nearest-neighbor gaussian process models for large geostatistical datasets. *Journal of the American Statistical Association*, 111(514):800–812, April 2016.
13. Oliver Hamelijnck, William J. Wilkinson, Niki A. Loppi, Arno Solin, and Theodoros Damoulas. Spatio-temporal variational gaussian processes. 11 2021.
14. Grant D. Brown, Aaron T. Porter, Jacob J. Oleson, and Jessica A. Hinman. Approximate bayesian computation for spatial seir(s) epidemic models. *Spatial and Spatio-temporal Epidemiology*, 24:27–37, February 2018.
15. Laís Picinini Freitas, Alexandra M. Schmidt, William Cossich, Oswaldo Gonçalves Cruz, and Marilia Sá Carvalho. Spatio-temporal modelling of the first chikungunya epidemic in an intra-urban setting: The role of socioeconomic status, environment and temperature. *PLOS Neglected Tropical Diseases*, 15(6):e0009537, June 2021.
16. Jifan Li, Edward L. Ionides, Aaron A. King, Mercedes Pascual, and Ning Ning. Inference on spatiotemporal dynamics for networks of biological populations. 11 2023.
17. Umberto Simola, Jessi Cisewski-Kehe, Michael U Gutmann, and Jukka Corander. Adaptive approximate bayesian computation tolerance selection. *Bayesian analysis*, 16(2):397–423, 2021.
18. Sen Pei, Sasikiran Kandula, Wan Yang, and Jeffrey Shaman. Forecasting the spatial transmission of influenza in the united states. *Proceedings of the National Academy of Sciences*, 115(11):2752–2757, February 2018.
19. Zhibin Shi, Lili Wei, Pengfei Wang, Shida Wang, Zaisi Liu, Yongping Jiang, and Jingfei Wang. Spatio-temporal spread and evolution of influenza a (h7n9) viruses. *Frontiers in Microbiology*, 13, September 2022.
20. Hawre Jalal, Kyueun Lee, and Donald S. Burke. Oscillating spatiotemporal patterns of covid-19 in the united states. *Scientific Reports*, 14(1), September 2024.
21. W. O. Kermack and A. G. McKendrick. A contribution to the mathematical theory of epidemics. *Proceedings of the Royal Society of London. Series A, Containing Papers of a Mathematical and Physical Character*, 115(772):700–721, 1927.
22. W. Marijn van Ballegooijen and Maarten C. Boerlijst. Emergent trade-offs and selection for outbreak frequency in spatial epidemics. *Proceedings of the National Academy of Sciences*, 101(52):18246–18250, December 2004.
23. Roy M Anderson and Robert M May. *Infectious Diseases of Humans: Dynamics and Control*. Oxford University Press, 05 1991.

24. Christoph Feichtenhofer, Yanghao Li, Kaiming He, et al. Masked autoencoders as spatiotemporal learners. *Advances in neural information processing systems*, 35:35946–35958, 2022.
25. Irina Higgins, Loic Matthey, Arka Pal, Christopher Burgess, Xavier Glorot, Matthew Botvinick, Shakir Mohamed, and Alexander Lerchner. beta-vae: Learning basic visual concepts with a constrained variational framework. In *International conference on learning representations*, 2017.
26. Jacob Devlin, Ming-Wei Chang, Kenton Lee, and Kristina Toutanova. Bert: Pre-training of deep bidirectional transformers for language understanding. In *Proceedings of the 2019 conference of the North American chapter of the association for computational linguistics: human language technologies, volume 1 (long and short papers)*, pages 4171–4186, 2019.
27. Kaiming He, Xinlei Chen, Saining Xie, Yanghao Li, Piotr Dollár, and Ross Girshick. Masked autoencoders are scalable vision learners. 11 2021.
28. Zhan Tong, Yibing Song, Jue Wang, and Limin Wang. Videomae: Masked autoencoders are data-efficient learners for self-supervised video pre-training. 03 2022.
29. Michael D McKay, Richard J Beckman, and William J Conover. A comparison of three methods for selecting values of input variables in the analysis of output from a computer code. *Technometrics*, 42(1):55–61, 2000.
30. Jean-Michel Marin, Pierre Pudlo, Christian P Robert, and Robin J Ryder. Approximate bayesian computational methods. *Statistics and computing*, 22(6):1167–1180, 2012.
31. Alfred James Lotka. *Elements of physical biology*. Williams & Wilkins, 1925.
32. Vito Volterra. Variations and fluctuations of the number of individuals in animal species living together. *ICES Journal of Marine Science*, 3(1):3–51, 1928.
33. Dennis Prangle. Adapting the abc distance function. 2017.
34. Khanh N Dinh, Zijin Xiang, Zhihan Liu, and Simon Tavaré. Approximate bayesian computation sequential monte carlo via random forests. *arXiv preprint arXiv:2406.15865*, 2024.
35. Bai Jiang, Tung-Yu Wu, Charles Zheng, and Wing H. Wong. Learning summary statistic for approximate bayesian computation via deep neural network. *Statistica Sinica*, 27(4):1595–1618, 2017.
36. Mattias Åkesson, Prashant Singh, Fredrik Wrede, and Andreas Hellander. Convolutional neural networks as summary statistics for approximate bayesian computation. *IEEE/ACM Transactions on Computational Biology and Bioinformatics*, 19(6):3353–3365, 2021.
37. Meili Baragatti, Casenave Céline, Bertrand Cloez, David Métivier, and Isabelle Sanchez. Approximate bayesian computation with deep learning and conformal prediction. 06 2024.

38. Paul Fearnhead and Dennis Prangle. Constructing summary statistics for approximate bayesian computation: Semi-automatic approximate bayesian computation. *Journal of the Royal Statistical Society Series B: Statistical Methodology*, 74(3):419–474, 05 2012.
39. Jiaquan Wang, Yang Zeng, Xinchao Jiang, Hu Wang, Enying Li, and Guangyao Li. Variational auto-encoder based approximate bayesian computation uncertain inverse method for sheet metal forming problem. 07 2019.
40. Stephan Rabanser, Tim Januschowski, Valentin Flunkert, David Salinas, and Jan Gasthaus. The effectiveness of discretization in forecasting: An empirical study on neural time series models. *arXiv preprint arXiv:2005.10111*, 2020.
41. Abdul Fatir Ansari, Lorenzo Stella, Caner Turkmen, Xiyuan Zhang, Pedro Mercado, Huibin Shen, Oleksandr Shchur, Syama Rangapuram, Sebastian Pineda Arango, Shubham Kapoor, et al. Chronos: Learning the language of time series. 2024.
42. David Salinas, Valentin Flunkert, Jan Gasthaus, and Tim Januschowski. Deepar: Probabilistic forecasting with autoregressive recurrent networks. *International journal of forecasting*, 36(3):1181–1191, 2020.

Supplementary Information

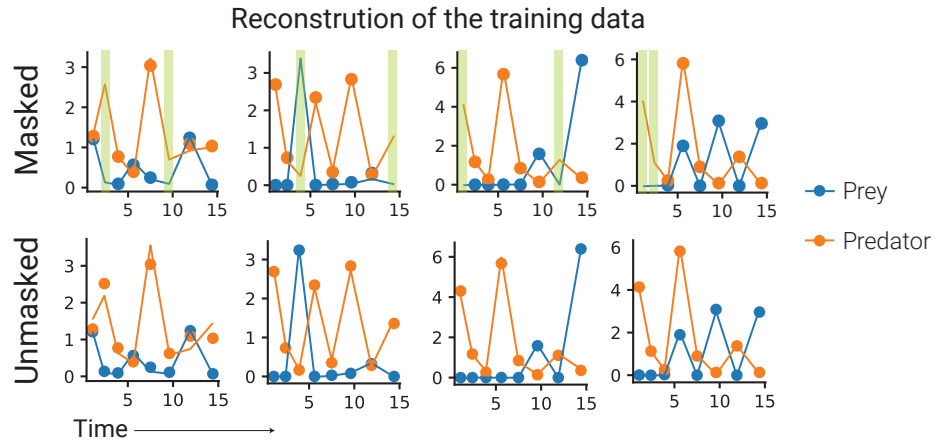


Figure S1: Masking Approach for the Lotka-Volterra model. Comparison of reconstructions from masked and unmasked inputs. Four randomly selected training samples are shown, with masked inputs in the first row and unmasked inputs in the second row. For each sample, $\approx 15\%$ of the data is masked at random (*i.e.* 2 data points) of the input is masked. Green bars indicate the positions of the masked data points. Lines represent the reconstructions of the original input shown as black dots.

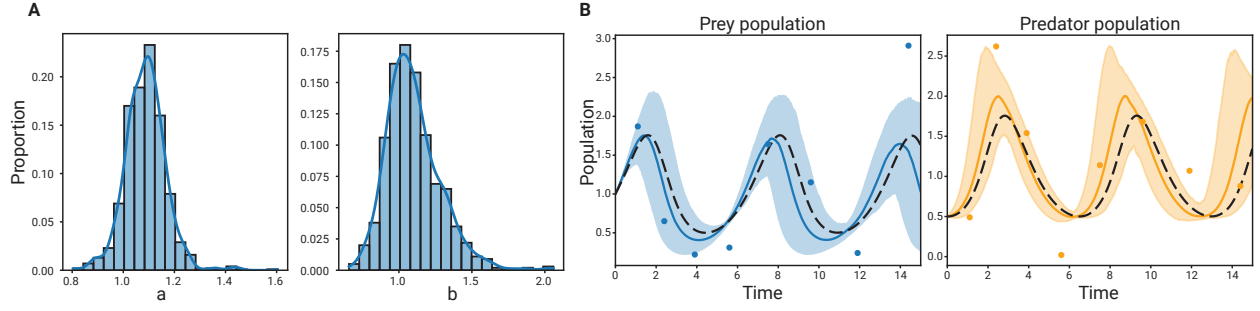


Figure S2: Inferring predator-prey dynamics using MCMC. **A.** Posterior distribution of parameters a and b using 1,000 accepted particles from MCMC for the Lotka-Volterra system. **B.** Predicted predator-prey dynamics with 95% credible intervals (shaded), and median trajectories (solid lines). Black dashed lines represent the ground truth dynamics.